



Improved short-term stability for real-time GNSS satellite clock estimation with clock model

Shengfeng Gu¹ · Feiyu Mao¹ · Xiaopeng Gong¹ · Yidong Lou¹ · Chuang Shi^{2,3}

Received: 30 June 2022 / Accepted: 6 May 2023 / Published online: 22 June 2023
© Springer-Verlag GmbH Germany, part of Springer Nature 2023

Abstract

As a basic service of global navigation satellite system (GNSS), the timing technique tends to be processed based on precise point positioning (PPP) with the advantages of convenience and high-precision combined. The increasing demand for real-time PPP promotes the development of real-time satellite clock estimation. In real-time satellite clock estimation, the phase white noise model is widely adopted. Nevertheless, the white noise may mask the short-term characteristic of satellite atomic clocks, thus affecting the performance of the timing service. Therefore, we developed a clock model to characterize atomic clocks for GPS, GLONASS, BDS, and Galileo satellites based on Hadamard deviation analysis of 90-week multi-GNSS final clock products generated from GeoForschungsZentrum (GFZ). The results suggest that GPS Block IIF/III, BDS-3, and Galileo clocks have relatively outstanding frequency stabilities. And for the product of these satellite clocks, the simulated real-time clock estimation indicates that the clock model can provide better stabilities than the white noise model and even GFZ final products. Moreover, the clock model can provide a short-term prediction service during the period of data interruption and accelerate the convergence of clock offsets once the data recovered in real-time applications. Finally, PPP one-way timing was performed with five MGEX stations linked with external time sources. When employing the clock products with the clock model, the average improvement rates in stabilities over intervals from 30 to 10,260 s are 59.8%, 68.2%, 74.7%, and 66.6% for GPS, GLONASS, BDS-3, and Galileo PPP one-way timing, respectively, in comparison with that of the white noise model.

Keywords Atomic clock model · Real-time · Clock estimation · PPP one-way timing

1 Introduction

GNSS provides services based on measuring signal travel time from satellites to the receiving user. To indicate the moment of signal transmitting accurately, the space-qualified atomic clock, which is relatively stable, is required for the timekeeping in the GNSS satellite (Beard and Senior 2017). Inversely GNSS plays a critical role in time and

frequency, such as accurate time dissemination and comparing clocks, particularly for the distant clocks (Defraigne 2017). GNSS time transfer is an effective technique to measure the time synchronization error between remote clocks as needed to realize Universal Time Coordinated (UTC). Due to the existence of ambiguities in carrier-phase data, conventional methods, including common-view (CV) and all-in-view (AV), are employed only using pseudorange measurements (Allan and Weiss 1980; Petit and Jiang 2008).

Precise point positioning (PPP) (Zumberge et al. 1997; Kouba and Héroux 2001) uses both pseudorange and phase observations, utilizing precise orbit and clock products to enable single-receiver users to determine their positions, clock synchronization errors, and tropospheric zenith delays with satisfactory accuracy. Although absolute time can only be obtained by the pseudorange observation, phase data with the benefit of low noise provide high-precision frequency information making PPP time transfer are currently widespread. It has been proved that PPP time transfer allows

✉ Xiaopeng Gong
xpgong@whu.edu.cn

¹ GNSS Research Center, Wuhan University, Luoyu Road 129, Wuhan 430079, Hubei, China

² Research Institute for Frontier Science, Beihang University, 37 Xueyuan Road, Beijing 100083, China

³ Laboratory of Navigation and Communication Fusion Technology, Ministry of Industry and Information Technology, Beijing 100083, China

remote clock comparisons to reach the precision at the sub-ns level using International GNSS Service (IGS) final products (Orgiazzi et al. 2005). Also, some researches present the comparison of time transfer performance with methods from CV, AV to PPP, ambiguity-fixed PPP (Verhasselt and Defraigne 2019; Ren et al. 2023). However, IGS final products and precise products generated by IGS analysis centers (AC) are post-processed and thus have various latencies from several to tens of days, limiting real-time application. To meet the increasing demand for applications requiring real-time high-precision products, the IGS has formally launched the real-time service (RTS) in April 2013 (Agrotis et al. 2017; Yang et al. 2019). This service offers users worldwide real-time orbit and clock corrections with latencies of a few seconds. With the above products, (near) real-time PPP time transfer experiments reveal a sub-ns precision as well (Cerretto et al. 2011; Defraigne et al. 2015). In addition to time transfer, PPP is applied in one-way timing as needed for the wide-area accurate time dissemination (Guo et al. 2019).

The accuracy of satellite orbit and clock corrections as the most crucial factor considerably determines the performance of PPP. For single-frequency users or uncombined model, ionospheric models (e.g., global ionosphere map) are also fundamental to account for significant ionospheric delays (van Bree and Tiberius 2012; Gu et al. 2015). Satellite orbit products that meet the requirement of PPP can be predicted for real-time applications. For instance, IGS ultra-rapid (IGU) products provide predicted GPS orbits with an accuracy of about 5 cm. Unfortunately, satellite clocks exhibit intense stochastic behaviors, periodic variations (Senior et al. 2008; Montenbruck et al. 2012) and even anomalies such as phase jumps, frequency steps (Beard and Senior 2017), and oscillation observed on the first two Galileo In-Orbit Validation (IOV) satellites due to a leakage of signals between two synthesizer chains (Montenbruck et al. 2017), which restricts the accuracy of predicted clocks resulting in approximate 30 times enlargement of the STD value for predicted versus observed portion in IGU clocks. Consequently, real-time clock estimation is a key point for high-precision GNSS service. At present, the phase white noise model is widely adopted in clock estimation of different IGS analysis centers (IGS ACs), such as Geo-ForschungsZentrum (GFZ), Wuhan University (WHU) and Centre National d'Etudes Spatiales (CNES) (https://igs.org/mgex/data-products/#orbit_clock). It seems to be sufficient for providing a centimeter-level positioning (Bock et al. 2009). Nevertheless, the white noise may mask the short-term characteristic of satellite atomic clocks and further affect the performance of the timing service. Extensive publications focusing on atomic frequency standard has brought abundant

knowledge about noise analysis (Allan 1987), performance evaluation (Vannicola et al. 2010), clock modeling (Stein and Filler 1988), etc. Multi-state clock model including phase, frequency, and drift is essential for time and frequency metrology. Previously owing to the IGS combined clock product being referenced to GPS time (GPST) by daily linear alignment separately, large offsets in time and frequency appear in the boundary between days. An IGS timescale (IGST) is developed to address this matter (Senior et al. 2003; Senior 2012). The ensemble algorithm uses a Kalman filter to maintain a stable timescale based on both ground and GPS satellite atomic clocks. The states of clocks are propagated between epochs with a multi-state clock model and updated using measurements of clocks relative to a reference clock. In addition to the property of continuity across days, another primary benefit of the algorithm is that it provides a quite stable ensemble reference. Center for Orbit Determination in Europe (CODE) performs ambiguity-fixed clock estimation and utilizes the integer-cycle recovery to remove day-boundary discontinuities. Also, an algorithm of real-time clock estimation with the clock model was presented by Hauschild and Montenbruck (2009), but the process noise parameters were regarded as identical for all satellite clocks. Currently, satellite clocks exhibit different performance in comparison between constellations and even between generations. Thus, the strategy of respective noise models for each satellite clock is supposed to be more appropriate. In real-time processing, data transmission may be interrupted resulting in clock jump when the white noise model is adopted. In the research of Shi et al. (2019), the clock model determined by the method of variogram can improve the performance of clock estimation when data are discontinuous compared with the white noise model; one drawback of this model is that all statistical noises of clock states are blended together and added in the phase, which is inaccurate for frequency and drift statistical model. Therefore, we determined clock models according to the characteristic of clocks and used the models in real-time clock estimation. The clock model can improve the robustness of clock offsets when data are discontinuous and their frequency stabilities. Furthermore, the clock products with modeling applied in time service can enhance the stabilities of one-way timing.

This paper starts with an introduction to the multi-GNSS data processing model and the clock model, followed by the evaluation of various atomic clocks and the determination of their stochastic noise level. Then, the data and software used in this study are described. Finally, the results of estimated clock products and PPP one-way timing are discussed. A brief summary is presented subsequently.

2 Observation equation and clock model

2.1 Ionosphere-free linear combination

The ionosphere-free (IF) combination is well-known for eliminating the effect of first-order ionospheric delay, thereby typically employed in satellite clock estimation. For the observation model in this paper, we assume the satellite positions are known, which means that they are computed from orbit products. Then, the linearized IF combination observation equations from satellite s to receiver r are given as follows:

$$\begin{aligned} \Delta p_{r,IF}^s &= -[e_r^s]^T \Delta r_r + \alpha_r^s \Delta T_r^z \\ &\quad + c \left(\Delta dt_{r,IF}^{sys} - \Delta dt_{IF}^s \right) + \varepsilon_{r,IF}^s \\ \Delta l_{r,IF}^s &= -[e_r^s]^T \Delta r_r + \alpha_r^s \Delta T_r^z \\ &\quad + c \left(\Delta dt_{r,IF}^{sys} - \Delta dt_{IF}^s \right) + \Delta \tilde{N}_{r,IF}^s + \eta_{r,IF}^s \end{aligned} \quad (1)$$

with

$$\begin{cases} \Delta p_{r,IF}^s = [\kappa^s]^T p_r^s - \left[\rho_r^s + \alpha_r^s T_r^z + c(dt_{r,IF}^{sys} - dt_{IF}^s) \right] \\ \Delta l_{r,IF}^s = [\kappa^s]^T l_r^s - \left[\rho_r^s + \alpha_r^s T_r^z + c(dt_{r,IF}^{sys} - dt_{IF}^s) - \tilde{N}_{r,IF}^s \right] \\ dt_{r,IF}^{sys} = dt_r + [\kappa^s]^T d_r^{sys} + [\kappa^s]^T O_{sys} \delta d_r^s \\ dt_{IF}^s = dt^s + [\kappa^s]^T d^s \\ \tilde{N}_{r,IF}^s = N_{r,IF}^s - c \left\{ [\kappa^s]^T (d_r^{sys} + O_{sys} \delta d_r^s + d^s) \right\} \\ \quad + c \left\{ [\kappa^s]^T (b_r^{sys} + O_{sys} \delta b_r^s + b^s) \right\} \end{cases} \quad (2)$$

where $\Delta p_{r,IF}^s$, $\Delta l_{r,IF}^s$ are observed-minus-calculated (OMC) pseudorange and phase observables in units of meters; the constellation identifier $sys \in \{G, R, C, E\}$ represents GPS, GLONASS, BeiDou (BDS), Galileo hereafter in agreement with the RINEX convention; the symbol Δ in the right side of Eq. (1) denotes corrections; e_r^s denotes the unit vector of line-of-sight, $r_r = [x_r \ y_r \ z_r]^T$ is the receiver coordinate vector; T_r^z is the zenith tropospheric delay with the mapping function α_r^s ; c is the speed of light in vacuum; $dt_{r,IF}^{sys}$, dt_{IF}^s are modified clock offsets absorbing combined code hardware delays for the receiver and satellite; $\tilde{N}_{r,IF}^s$ denotes modified ambiguity in units of length; $\varepsilon_{r,IF}^s$ and $\eta_{r,IF}^s$ are random noise for pseudorange and phase, respectively; IF combination coefficient vector for f_1 and f_2 frequencies is denoted as $\kappa^s = \left[\frac{f_1^2}{f_1^2 - f_2^2} \ - \frac{f_2^2}{f_1^2 - f_2^2} \right]^T$, which is generally the same for satellites in a constellation based on code division multiple access (CDMA) except GLONASS based on frequency division multiple access (FDMA); the rest of bold symbols refers to a two-dimensional vector consisting of counterparts in f_1 and f_2 ; p_r^s , l_r^s are observations for pseudorange and phase; ρ_r^s is the geometry distance after correcting effects of the antenna

phase center offset (PCO) and variation (PCV), phase wind-up, relativity, solid earth and ocean tide; dt_r and dt^s are actual clock offsets for the receiver and satellite, respectively; $N_{r,IF}^s$ denotes float IF combination ambiguity in units of length; d_r^{sys} and b_r^{sys} are receiver code and phase hardware biases for sys , as well as d^s and b^s for the satellite; at last, δd_r^s and δb_r^s are code and phase inter-channel biases accounting for the FDMA technology, the corresponding coefficient O_{sys} is related to the constellation

$$O_{sys} = \begin{cases} 0, & CDMA : G, C, E \\ 1, & FDMA : R \end{cases} \quad (3)$$

Note that δd_r^s is usually calculated in advance for calibration in GLONASS precise data processing, otherwise the common receiver clock offset of GLONASS we described is inappropriate and the model is hard to resolve. The satellite clock offset based on the IF combination solution assimilates combined code biases because of the strong correlation between parameters. Similarly, prepared differential code biases (DCBs) are applied to avoid the effect of intra-frequency code bias such as C/A and P1 codes in the first frequency of GPS, so that consistent code biases (G: P1/P2, R: P1/P2, C: B1I/B3I, E: E1/E5a) are included in clock offsets and processed in PPP. Moreover, the apparent code bias variation for BDS-2 and receiver-type-related code signal distortion biases are removed based on the researches of Lou et al. (2017) and Gong et al. (2022), respectively. In Eq. (1), the correction items can be omitted provided that they are recognized as known values by the use of other products, e.g., IGS weekly coordinate solution for the receiver position.

Last but not least, extra constraints, also called datum, are required to cope with the linear dependence of the satellite and the receiver clock offset. In this study, the following constraint

$$\sum_{s=1}^j \Delta dt_{IF}^s = 0, \quad (4)$$

is introduced for each constellation and each epoch in the white noise model. Additionally, each clock estimate is referenced to a linear alignment to the underlying system time in the broadcast ephemeris (BRDC) per epoch. Nevertheless, the linear alignment adjusts the datum of clock products per epoch with a poor performance, which is affected by the low accuracy of broadcast ephemeris and will destroy the model of atomic clocks. For this reason, the gravity datum is just adopted in the first epoch for the clock model, and subsequently virtual observations of compensating for the difference between the datum of the estimated clock and the

underlying system time in the broadcast ephemeris

$$\sum_{s=1}^j (\Delta dt_{IF}^s)_k = \sum_{s=1}^j (dt_{IF, BRDC}^s - dt_{IF}^s)_{k-1}, \tag{5}$$

are selected as weak constraints (the same weight as a full-weight IF pseudorange observation) so as not to deviate enormously from the system time. After obtaining estimated clocks dt_{IF}^s and broadcast clocks $dt_{IF, BRDC}^s$ at epoch $k - 1$, the right side of Eq. (5) can be calculated. Then, the above constraint equation is added at the next epoch k .

2.2 Satellite clock model

The clock states evolve from epoch t_{k-1} to the next t_k can be written as

$$\mathbf{x}_k = \Phi(t_k, t_{k-1})\mathbf{x}_{k-1} + \boldsymbol{\omega}(t_k, t_{k-1}) \tag{6}$$

where $\mathbf{x}(t) = [p(t) \ f(t) \ r(t)]^T$ is a three-state vector of the clock offset including the phase offset $p(t)$, the frequency offset $f(t)$ and the frequency drift offset $r(t)$; the state transform matrix Φ for the time step $\delta = t_k - t_{k-1}$ is

$$\begin{aligned} \Phi(t_k, t_{k-1}) &= \begin{pmatrix} 1 & t_k - t_{k-1} & (t_k - t_{k-1})^2/2 \\ 0 & 1 & t_k - t_{k-1} \\ 0 & 0 & 1 \end{pmatrix} \\ &= \begin{pmatrix} 1 & \delta & \delta^2/2 \\ 0 & 1 & \delta \\ 0 & 0 & 1 \end{pmatrix} \end{aligned} \tag{7}$$

and let $\boldsymbol{\xi}(t) = [\xi_p \ \xi_f \ \xi_r]^T$ denotes the noise vector consisting of random walk noise in phase, frequency, and drift; assuming the three noise processes are independent, then the stochastic model of random disturbance $\boldsymbol{\omega}(t_k, t_{k-1}) = \int_{t_{k-1}}^{t_k} \Phi(t_k, t)\boldsymbol{\xi}(t)dt$ can be expressed as the following

$$\begin{cases} E[\boldsymbol{\omega}(t_k, t_{k-1})] = 0 \\ D[\boldsymbol{\omega}(t_k, t_{k-1})] \\ = \begin{pmatrix} S_p\delta + S_f\delta^3/3 + S_r\delta^5/20 & S_f\delta^2/2 + S_r\delta^4/8 & S_r\delta^3/6 \\ S_f\delta^2/2 + S_r\delta^4/8 & S_f\delta + S_r\delta^3/3 & S_r\delta^2/2 \\ S_r\delta^3/6 & S_r\delta^2/2 & S_r\delta \end{pmatrix} \end{cases} \tag{8}$$

where S_p, S_f , and S_r are individual spectral densities of noise processes in $\boldsymbol{\xi}(t)$.

3 Stochastic model of GNSS satellite clock

In this section, the multi-GNSS precise clock products generated by the GFZ during a 90-week period from the GPS week 2087 to 2176 (day of year (DOY) 005, 2020—DOY 268, 2021) are utilized to evaluate the stability and further determine the stochastic model of GNSS satellite clocks.

3.1 GNSS satellite clock stability

The Institute of Electrical and Electronics Engineers (IEEE) has recommended the two-sample deviation, named Allan deviation (the square root of Allan variance), to define the frequency stability. However, the Allan deviation will be affected by linear frequency drift for some clocks, e.g., rubidium (Rb) atomic clocks. The effect is typically dominant in intervals of longer than 1 day (Hutsell et al. 1996). As a result, the linear frequency drift must be removed prior to analyzing the clock stability using Allan deviation. Alternatively, the three-sample deviation, referred to as Hadamard deviation (HDEV), has the advantage of automatically removing linear frequency drift, which makes it particularly appropriate for the analysis of Rb atomic clocks. Various technologies about frequency stability analysis have been summarized in the book by Riley and Howe (2008), among them the overlapping Hadamard deviation can make maximum use of a data set by overlapping samples making the confidence of estimation increased greatly, and was adopted in this paper. The overlapping Hadamard deviation can be estimated from phase (time) measurements by the following expression

$$\begin{aligned} H\sigma_y^2(\tau) &= \frac{1}{6\tau^2(N - 3m)} \\ &\times \sum_{i=1}^{N-3m} [x_{i+3m} - 3x_{i+2m} + 3x_{i+m} - x_i]^2 \end{aligned} \tag{9}$$

where $H\sigma_y^2(\tau)$ denotes the Hadamard variance; $\tau = m\tau_0$ is the averaging interval, in which m is the averaging factor and τ_0 is the basic measurement interval; x_i is the i th in the phase series consisting of N values. In addition, the Hadamard deviation $H\sigma_y$ is a more common expression.

The 90-week precise products include the effects of abnormalities and adjustments of satellite clocks, clock/satellite replacement, etc. Consequently, a series of pre-processions are necessary before estimating the Hadamard deviation. The frequency data formed by the differenced values of adjacent phase measurements were employed to detect and eliminate gross errors by the median absolute deviation (MAD) method, and the procedure is carried out for separate days so that the frequency drift is convenient to deal with and can be ignored directly in one day. Meanwhile, the satellite clock offsets may exhibit day-boundary discontinuities

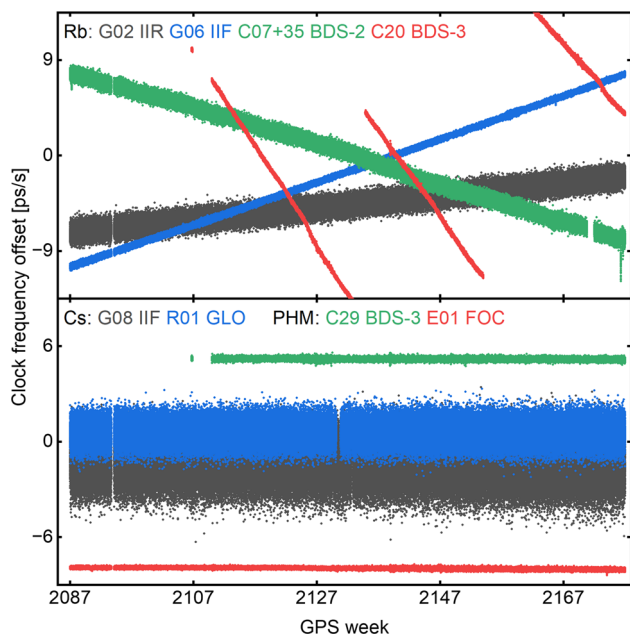


Fig. 1 Satellite clock frequency offset over GPS week 2087–2176. + 35 ps/s were added in the frequency offsets of C07

or phase adjustments, which were detected and removed by phase extrapolation based on the frequency data. For frequency adjustments or clock/satellite replacement, the clock products were divided into separate periods to estimate the Hadamard deviation. The HDEV of long-term intervals is unable to be estimated due to the short-period data of the new clocks/satellites.

Figure 1 gives the frequency data of eight satellite clocks for the period of 90 weeks. In the top plot, four Rb clocks exhibit apparent linear frequency drift, while no obvious drift can be found for Cs and PHM clocks in the bottom plot. Note that + 35 ps/s were added in the frequency offsets of C07. In addition, the Rb clocks of G06 (Block IIF) and C20 (BDS-3) show less noise in frequency compared with that of G02 (Block IIR) and C07 (BDS-2). Considering that the Cs and PHM clocks have no obvious linear frequency drift, we simplified the model of these clocks to a two-state clock model just consisting of the phase and frequency.

Figure 2 presents the overlapping HDEV of satellite clocks for GPS, GLONASS, BDS, and Galileo over the averaging intervals from 30 to about 5×10^6 s. According to the HDEV characteristics, the GPS satellite clocks were divided into three groups including Rb clocks for Block IIR/IIR-M, Rb clocks for Block IIF/III, and one cesium (Cs) clock of the Block IIF satellite SVN72 (PRN G08). Note that the Block IIF satellite SVN65 (PRN G24) is switched from a Cs to a Rb clock between DOY 112 and 113, 2021, which is described in GPS operational advisory (OA) files (<https://www.navcen.uscg.gov/sites/default/files/>

[gps/opsadvisory/2021/](https://www.navcen.uscg.gov/sites/default/files/gps/opsadvisory/2021/)). Moreover, the satellite replacement was implemented for some signals, e.g., PRN G11 and PRN G23. Only the results of the new clocks/satellites are shown. It is easily noticed that the latest Rb clocks installed on IIF/III satellites show a significant improvement in stability for averaging intervals from 30 to 10,000 s compared with IIR/IIR-M Rb clocks, even have an order of magnitude smaller in HDEV. Also, GPS satellite clocks of the same generation have virtually identical performance, which is similar for both BDS-3 Rb and passive hydrogen maser (PHM) clocks, as well as Galileo PHM clocks equipped on full operational capability (FOC) and IOV satellites. In contrast, an obvious disparity in HDEV was observed for Cs clocks equipped on GLONASS satellites and Rb clocks equipped on BDS-2 satellites. Comparing the results of different constellations, the stability performance of IIF/III Rb clocks, both BDS-3 Rb and PHM clocks, and Galileo PHM clocks seems to be comparable, for which the decreasing range of average HDEV over averaging intervals between 30 and 100,000 s is $239.3\text{--}7.2 \times 10^{-15}$, $301.9\text{--}14.5 \times 10^{-15}$ and $201.0\text{--}7.6 \times 10^{-15}$, respectively. The stabilities of BDS-3 clocks are improved greatly as well compared with BDS-2 Rb clocks. Additionally, most satellite atomic clocks exhibit more complex behavior and have an increased HDEV due to the effect of periodic clock variations as pointed out by Senior et al. (2008) and Montenbruck et al. (2012), but Cs atomic clocks seem to be less affected.

3.2 Stochastic model determination

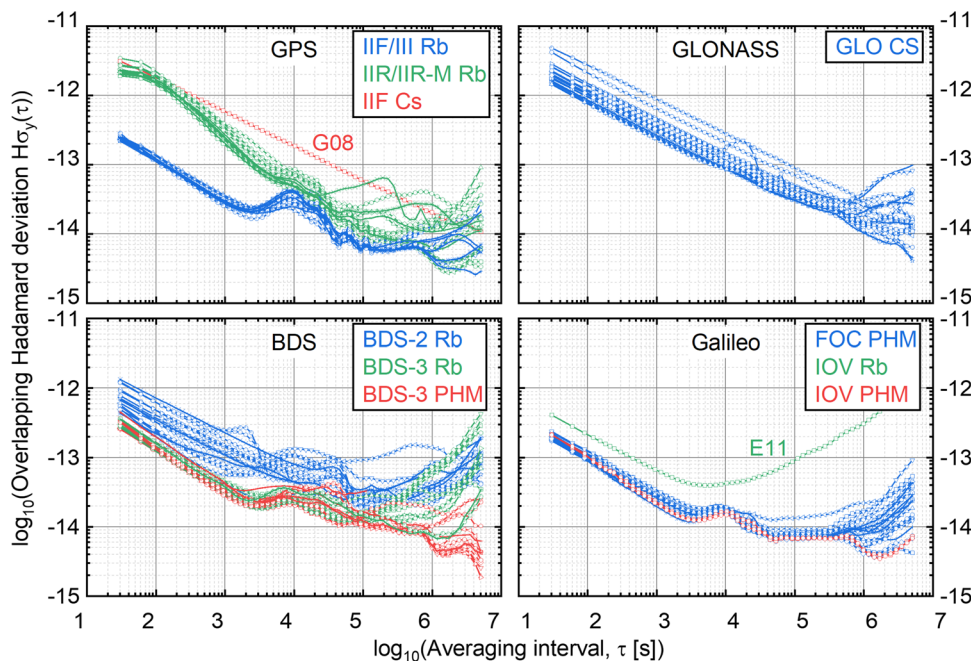
The spectral density parameters in Eq. (8) characterize the stochastic properties of the clock, which are key for the clock model. For the determination of spectral densities, the analysis of Allan variance and Hadamard variance provides a useful method. In the presence of both three noise types in Eq. (8) and white noise over phase, the relationship between Hadamard variance $H\sigma_y^2(\tau)$ and spectral density values has been established by Hutsell (1995) as the following equation

$$H\sigma_y^2(\tau) = \frac{10}{3}S_\theta\tau^{-2} + S_p\tau^{-1} + \frac{1}{6}S_f\tau + \frac{11}{120}S_r\tau^3 \quad (10)$$

where S_θ is the parameter designed for white noise over phase, also referred to as representation error. Note that S_θ is not all caused by the atomic clock itself, but also accounts for other effects such as errors in clock products. Consequently, it is not contained in the standard three-state model. We assume that the white phase noise of satellite clocks is introduced by the measurement noise.

Based on Eq. (10) together with the HDEV results, we determined the spectral density parameters for each constellation or generation by least square estimation (spectral density parameters can be obtained from the link: <https://www.navcen.uscg.gov/sites/default/files/gps/opsadvisory/2021/>).

Fig. 2 Overlapping Hadamard deviation of satellite clocks for GPS (top-left), GLONASS (top-right), BDS (bottom-left), and Galileo (bottom-right) based on GFZ multi-GNSS final clock products over GPS week 2087 to 2176, where the color indicates the generation of satellites or the type of clocks



[researchgate.net/project/Atomic-clock-model](https://www.researchgate.net/project/Atomic-clock-model)). The PHM clocks of Galileo IOV and FOC satellites were regarded as the same type due to their similar performance. Also, the random walk noise in drift is ignored for Cs and PHM clocks.

4 GNSS satellite clock estimation and PPP time transfer

In this section, simulated real-time clock estimation was performed with the white noise model and the clock model using the real-time stored observations and predicted orbit. Next, estimated clock products were utilized to investigate the performance of PPP one-way timing.

4.1 Data and processing strategy

The real-time GNSS observation data for the period of GPS week 2177–2183 (DOY 269–317 in 2021), collected and stored via the internet with the NTRIP protocol, were employed for simulated real-time clock estimation. Moreover, five Multi-GNSS EXperiment (MGEX) stations (Montenbruck et al. 2017) listed in Table 1, which were operated by a local time laboratory and supported by the corresponding real-time physical realization of UTC, named UTC(k), were selected to analyze the quality of time transfer based on PPP solution using estimated clock products under both the white noise and clock model. The station positions were fixed with the IGS weekly SNX file, and the distribution of GNSS tracking stations for clock estimation and time transfer experiment is illustrated in Fig. 3 marked as cir-

Table 1 Details of the stations used for PPP time transfer

Station	Time laboratory	Country	Satellite system
BRUX	ORB	Belgium	G + R + C + E
IENG	IT	Italy	G + R + C + E
PTBB	PTB	Germany	G + R + C + E
SPT0	SP	Sweden	G + R + C + E
USN8	USNO	USA	G + R + C + E

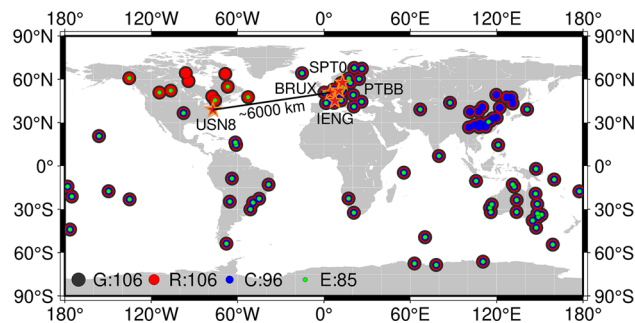


Fig. 3 Distribution of GNSS stations used for satellite clock estimation (circle) and time transfer (star), where the color indicates which constellation can be tracked for the station, and the digits on the left-bottom represent the numbers of corresponding stations

cles and stars, respectively. As for the satellite orbit, we utilized the predicted multi-GNSS orbit generated by the software PANDA to simulate a real-time setting. In addition, GLONASS Inter-channel biases were corrected based on the research by Zhang et al. (2021). For clock estimation, four satellite system (G, R, C, E) solutions were processed

Table 2 Information of the processing strategy and the parameters

Item	Strategy
Station coordinate	Fixed with IGS weekly SNX file, some stations located in China are not from IGS tracking networks and their positions are estimated in static mode
Satellite orbit	Fixed with predicted multi-GNSS orbit generated by PANDA software and updated per three hours (Guo et al. 2016)
Antenna phase center	igs14.atx
Elevation angle cutoff	7°
Interval	30 s
Weighting	3 dm for raw pseudorange and 3 mm for raw phase, low elevation (< 25°) observables are down-weighted
Receiver clocks	One clock parameter for each system as white noise process
Satellite clocks	(1) White noise and one clock parameter for each satellite, the gravity datum of broadcast ephemeris clock is selected as clock datum for each epoch (2) Clock model for each constellation/generation, the gravity datum of broadcast ephemeris clock is selected as clock datum at the first epoch
Troposphere	One zenith tropospheric delay for each station as random walk process
Ionosphere	Eliminated first-order delay with dual-frequency IF combination and ignored high-order delay
Ambiguity	Constant for each continuous arc

in one square root information filter (SRIF) day by day. For more details about the processing strategy, we refer to Table 2. All experiments are performed with the software, FUSing IN GnsS (FUSING), which is capable of high-precision real-time GNSS data processing (Dai et al. 2022), ionosphere and troposphere modeling (Zheng et al. 2018; Luo et al. 2020), and multi-sensor navigation (Gu et al. 2021).

4.2 Satellite clock estimation

The satellite clock estimation was conducted in a server with two Intel(R) Xeon(R) Gold 6128 CPUs of 3.40 GHz and a memory size of 125 GB. With the benefit of the blocked algorithm and optimized arrangement of parameters (Gong et al. 2018), a four-system clock estimation solution can be real-time processed and only takes about 3.65 and 3.84 s (average value of epochs for GPS week 2180–2181) per epoch for the

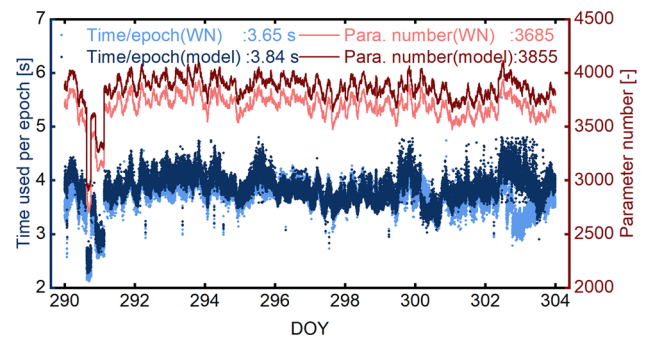


Fig. 4 Execution time per epoch (scatter points in blue) and parameter number (lines in red) for GPS week 2180–2181 (DOY 290–303, 2021). The results are plotted in light and dark color for the white noise (abbreviated as WN hereinafter) and clock model (abbreviated as model hereinafter), respectively

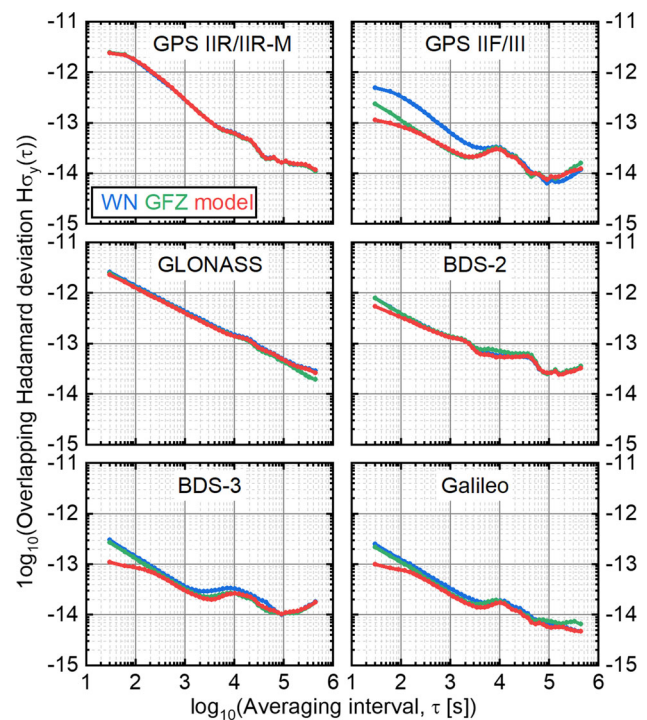


Fig. 5 Overlapping HDEV of the estimated clock products with the WN (blue) and model (red). Average values for different sets of clocks were calculated and plotted. Also, the results of GFZ final multi-GNSS products (green) for the same period were shown as references

white noise and clock model, respectively. The average numbers of parameters and measurements are 3,685/3,855 (white noise/clock model) and 5,720 per epoch (Fig. 4).

4.2.1 Stability and accuracy

To assess the stability of estimated clock products based on the white noise model and the proposed clock model, the HDEV of 7-week (i.e., GPS week 2177–2183) clock products was estimated over the averaging intervals from 30 to

Table 3 Overlapping HDEV ($\times 10^{-12}$) of clock products for averaging intervals 30, 60 and 90 s

System/Generation	WN	GFZ	Model
	30/60/90 s	30/60/90 s	30/60/90 s
GPS IIR/IIR-M	2.430/2.179/1.806	2.467/2.238/1.862	2.379/2.199/1.844
GPS IIF/III	0.489/0.420/0.353	0.235/0.158/0.121	0.114/0.099/0.088
GLONASS	2.602/1.794/1.454	2.456/1.695/1.373	2.319/1.631/1.331
BDS-2	0.798/0.528/0.420	0.790/0.523/0.415	0.541/0.413/0.350
BDS-3	0.304/0.194/0.153	0.271/0.177/0.139	0.109/0.094/0.088
Galileo	0.253/0.165/0.132	0.216/0.144/0.117	0.100/0.084/0.079

Table 4 Average RMS/STD values (ns) of estimated clock products

System/Generation	WN		Model	
	RMS	STD	RMS	STD
GPS IIR/IIR-M	0.489	0.076	0.485	0.076
GPS IIF/III	0.529	0.076	0.527	0.076
GLONASS	1.098	0.229	1.099	0.227
BDS-2	0.806	0.197	0.783	0.189
BDS-3	0.671	0.103	0.679	0.103
Galileo	0.308	0.065	0.314	0.065

432,000 s (five days). For comparison, the HDEV of GFZ final products in the same time period was derived as well. And the results are depicted in Fig. 5. Corresponding values of HDEV for averaging intervals 30, 60 and 90 s are listed in Table 3. Moreover, the statistical RMS and STD values were obtained by comparing with GFZ final products, which are summarized in Table 4 after being averaged for each system/generation. It is interesting to note that the stabilities of estimated clock products with the clock model are improved more obviously for satellite clocks with outstanding stabilities such as clocks of GPS IIF/III, BDS-3, and Galileo satellites. The short-term stabilities of products with the clock model for these clocks even outperform that of GFZ final products, while they have a similar performance of stabilities for intervals longer than 300 s. Nevertheless, only a slight increase in the stability performance was found in short averaging intervals for GPS IIR/IIR-M, GLONASS, and BDS-2 satellite clocks. Meanwhile, the accuracy of clock products with both clock and white noise model are almost identical, which demonstrates the improvement of stabilities for the clock model will be harmless to the accuracy. During the experimental period, the predicted orbit for GLONASS appeared unhealthy frequently leading to a decrease in the accuracy of clock products. Even though the number of tracking stations for Galileo is the least, the performance of clock products seems to be the most excellent for both accuracy and stability.

4.2.2 Performance within undergoing data discontinuity

On the 6th day of GPS week 2177 (DOY 274 in 2021), most observation data were interrupted for about one and a half hours. There are just around fifteen stations that can be tracked in this period. Data interruption results in no continuous observation arc for some satellites and their clock estimation process has to be reinitialized. For the white noise model, all information of the satellite clock in the filter vanishes accompanied by reinitialization. However, the clock model can provide a short-term prediction service according to the estimated clock states. Meanwhile, state propagation with the clock model makes the clock offset be convergent more quickly once the data recovered.

Figure 6 presents the time series of clock offsets for G03, C22, E12, and E21 compared with GFZ final products. Also, the number of stations tracking the satellites is plotted in yellow. At around 1 a.m., data interruption starts and leads to the failure of clock estimation. The clock products with the white noise (blue) were interrupted accordingly, while the clock model (red) provides the predicted clock offsets with satisfying accuracy. Later, the clock products under the clock model for the four satellites return to normal rapidly with the recovery of data. Instead, the clock estimation of G03 and C22 is reinitialized and still not convergent after one and a half hours (time of initialization in the strategy). Although the clock solutions of E12 and E21 are not reinitialized (have continuous arcs), the clock offsets jump apparently and re-converge for a while. Additionally, the STD values of

Fig. 6 Comparison of the clock estimation under the WN (blue) and model (red) when data is discontinuous, the right y-axis shows the number of stations tracking each satellite

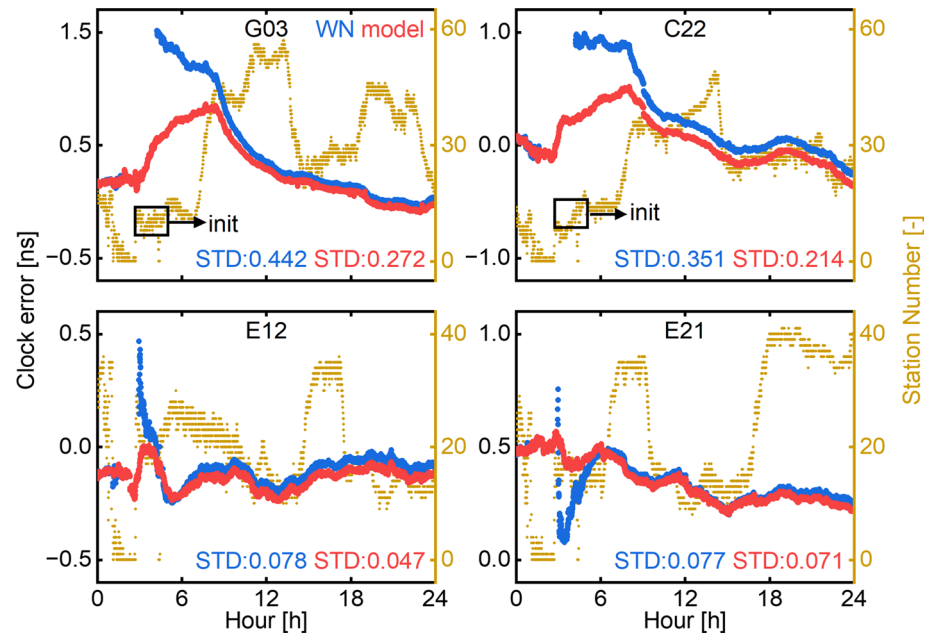


Table 5 Average STD values (ns) of estimated clock products for DOY 274 in 2021

System/Generation	WN	Model
GPS IIR/IIR-M	0.114	0.114
GPS IIF/III	0.121	0.115
GLONASS	0.380	0.362
BDS-2	0.106	0.105
BDS-3	0.149	0.141
Galileo	0.075	0.070

clock products decrease greatly and the average values of each system are presented in Table 5 for this day. Note that the predicted portion was excluded in the calculation of STD statistics.

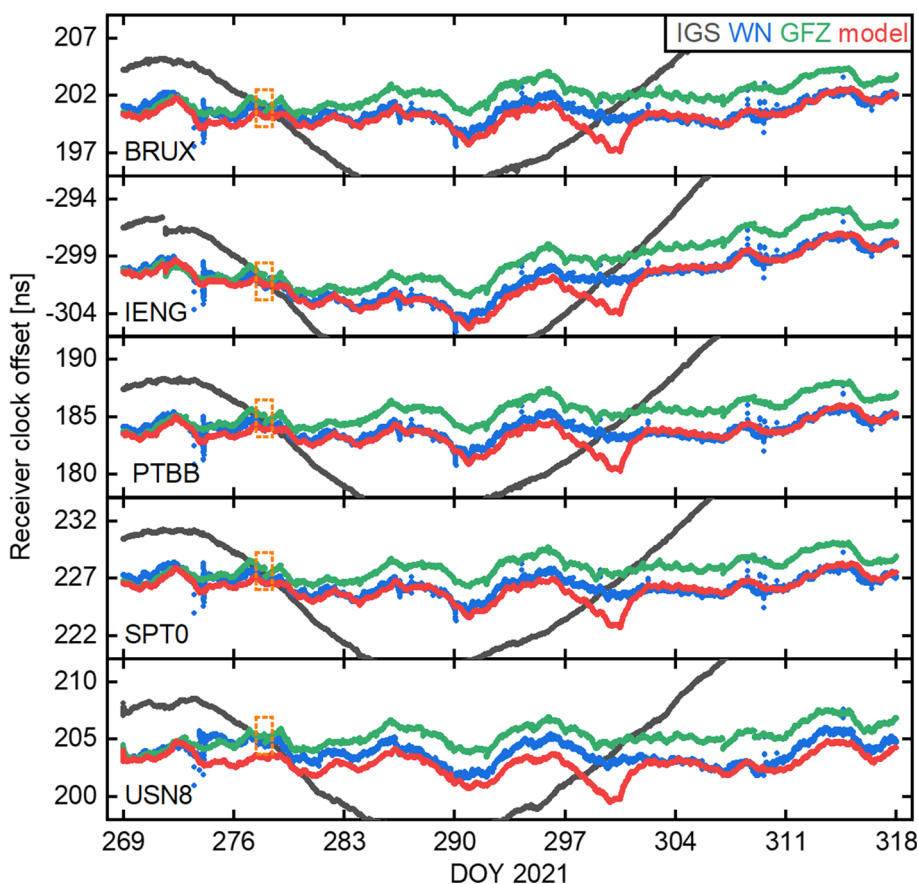
4.3 PPP one-way timing

Based on the estimated clock together with the predicted orbit, receiver clock offsets for each system of five stations with external time sources were estimated by PPP solution in static mode (fixed coordinates with the IGS weekly SNX file). Owing to the lack of satellites with the capability of providing global services, BDS-2 constellation was not investigated in this section. Although BDS-3 constellation can be tracked by the stations IENG and USN8, most observations in the second frequency are missing resulting in IF combination cannot be formed. Therefore, these two stations were excluded in the analysis of BDS-3 constellation.

Figure 7 presents the receiver clock offsets for each station based on GPS PPP solutions with various products: final products from IGS and GFZ MGEX analysis line, and predicted orbit and estimated clock products in our study. For the presentation of details about receiver clock offsets with PPP solutions, partial results of IGS exceed the scale range. Since the day-boundary discontinuities of GFZ final satellite clock products, receiver clock offsets exhibit an obvious jump (e.g., DOY 278 in 2021, inside orange rectangles). Whereas they are continuous for IGS final products assimilated to the IGST and solutions with the estimated satellite clocks, which are benefited from being processed day by day as mentioned in Sect. 4.1. Compared with the WN clock products, modeled satellite clocks make the results smoother and have few discrete points. The receiver clock offsets of all stations seem to have an extremely similar variation for solutions with the same products. It implies that the variation is most likely affected by the underlying datum of satellite clock offsets, which explains the differences between receiver clock offsets with different products. Apparent variations of receiver clock offsets from PPP solutions with IGS final products relative to that of other clock products reflect essentially the variations of IGST against other clock datum.

Concerning the stability of PPP one-way timing, corresponding HDEVs of the time series in Fig. 7 were estimated for averaging intervals between 30 and 86,400 s and illustrated in Fig. 8. Moreover, average HDEVs of estimated station clock offsets for GPS and other systems are shown in Fig. 9. PPP one-way timing with modeled clock products shows greatly increased stabilities compared with using WN clock products, especially in short-term intervals. For intervals from 30 to 10,260 s, the HDEVs in Fig. 8 for SPT0

Fig. 7 Time series of the receiver clock offsets obtained with GPS PPP solutions using final clock products from IGS (black) and GFZ (green), and estimated clock products under the WN (blue) and model (red)



decrease from $44.0\text{--}1.4 \times 10^{-14}$ to $18.0\text{--}0.9 \times 10^{-14}$, as well as the average rates of improvement in stabilities are 59.8%, 68.2%, 74.7%, and 66.6% for GPS, GLONASS, BDS-3, and Galileo, respectively. Owing to the problem of our predicted orbit of GLONASS, the corresponding performance of PPP was poor resulting in terrible stabilities of one-way timing in comparison with the results of GFZ final products (Fig. 9). However, the stabilities of PPP one-way timing with the products under modeling can reach a similar performance of that with GFZ final products for GPS, BDS-3, and Galileo. Although the estimated products with the clock model show better short-term stabilities than GFZ final products in Fig. 5, they provide similar stability performance of PPP one-way timing with the effect of PPP noise (Guo et al. 2022).

5 Conclusions

Satellite clock estimation is still the only effective way to deal with the clock offsets for real-time high-accuracy application of GNSS PPP at this stage. Considering that the white noise model widely adopted in GNSS satellite clock estimation probably masks the characteristics of clocks, we performed the simulated real-time multi-GNSS clock estimation with the clock model. Before this, the stabilities of satellite clocks

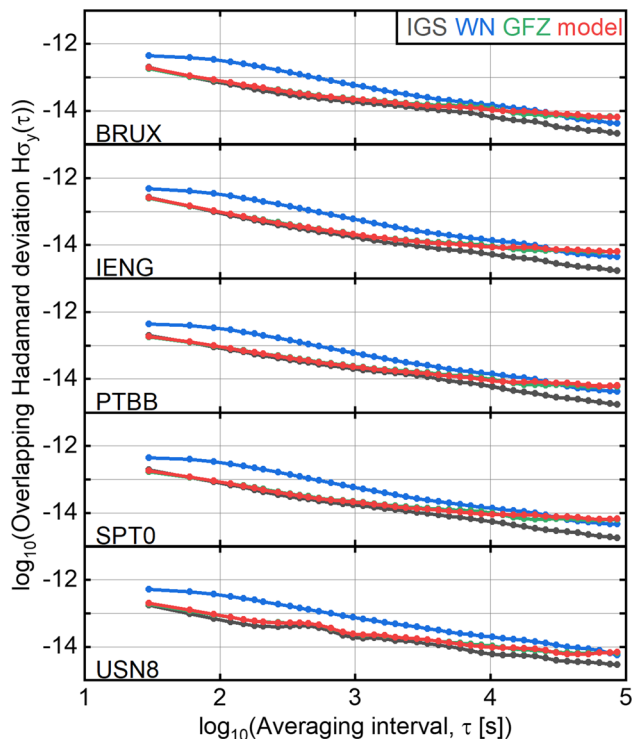


Fig. 8 Overlapping Hadamard deviation of the receiver clock offsets for GPS in Fig. 7. The data of this plot are given in Table 6 for averaging intervals 30, 1140 and 86,400 s

Fig. 9 Overlapping Hadamard deviation of receiver clock offsets for each system. HDEV values for stations were averaged and depicted according to the system. The data of this plot are given in Table 7 for averaging intervals 30, 1140 and 86,400 s

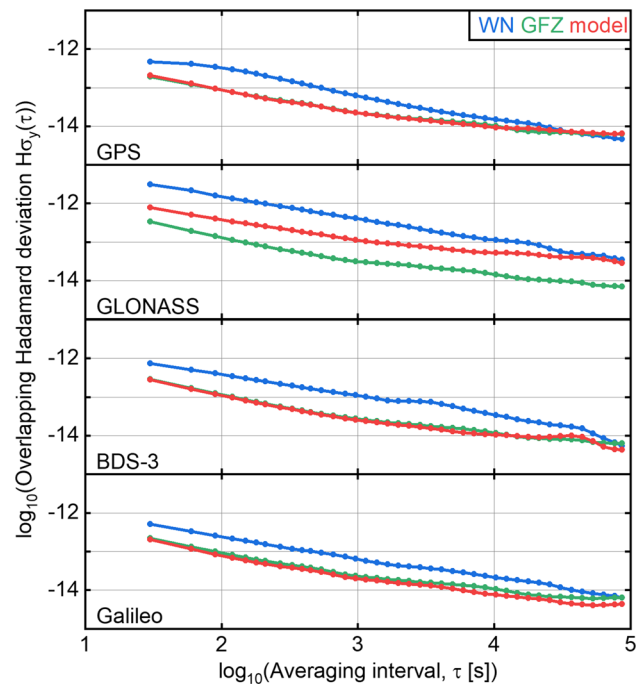


Table 6 The HDEV values ($\times 10^{-13}$) in Fig. 8 for averaging intervals 30, 1140 and 86,400 s

Products	BRUX 30/1140/86400 s	IENG 30/1140/86400 s	PTBB 30/1140/86400 s	SPT0 30/1140/86400 s	USN8 30/1140/86400 s
IGS	2.021/0.175/0.021	2.673/0.154/0.017	1.972/0.184/0.017	1.936/0.161/0.018	1.730/0.178/0.029
WN	4.433/0.525/0.041	4.764/0.518/0.045	4.418/0.532/0.043	4.396/0.520/0.046	5.236/0.677/0.055
GFZ	1.801/0.214/0.064	2.516/0.191/0.063	1.758/0.222/0.060	1.696/0.202/0.062	1.868/0.222/0.064
Model	1.963/0.209/0.065	2.594/0.191/0.064	1.874/0.214/0.063	1.804/0.195/0.066	2.004/0.225/0.068

Table 7 The HDEV values ($\times 10^{-13}$) in Fig. 9 for averaging intervals 30, 1140 and 86,400 s

Products	GPS 30/1140/86400 s	GLONASS 30/1140/86400 s	BDS-3 30/1140/86400 s	Galileo 30/1140/86400 s
WN	4.649/0.554/0.046	30.695/3.676/0.346	7.362/1.022/0.054	5.093/0.573/0.064
GFZ	1.928/0.210/0.062	3.354/0.295/0.069	2.890/0.254/0.062	2.182/0.217/0.064
Model	2.048/0.207/0.065	7.724/1.047/0.285	2.836/0.239/0.043	2.047/0.185/0.044

for four GNSS constellations (G, R, C, E) were evaluated with GFZ final clock products to determine the corresponding stochastic models. The results indicate that the estimated satellite clock products with modeling exhibit significantly improved stabilities compared with the white noise model in short-term averaging intervals for clocks of GPS IIF/III, BDS-3, and Galileo, which are the latest generation of satellite clocks and relatively more stable. Moreover, the clock model can provide short-term predicted clock products and accelerate the satellite clock estimation initialization when data interruption appears for real-time applications. Finally, the above clock products were employed in PPP one-way timing based on five MGEX stations operated by different time laboratories. When using the clock products with

the clock model against the white noise model, the rates of improvement in stabilities over intervals from 30 to 10,260 s are 59.8%, 68.2%, 74.7%, and 66.6% for GPS, GLONASS, BDS-3, and Galileo, respectively.

Acknowledgements Thanks for the data support of MGEX. This study is partially supported by the National Key Research and Development Plan (No. 2021YFB3900703), the National Natural Science Foundation of China (42274023, 41904016) and Young Elite Scientists Sponsorship Program by CAST (No. YESS20210184).

Author contributions GS and MF designed and performed this research; MF and GX analyzed data; MF wrote the paper; all authors provided critical feedback and reviewed the paper.

Data availability The multi-GNSS datasets analyzed during the current study are available from <ftp://igs.gnsswhu.cn/>.

Declarations

Conflict of interest The authors have no competing interests to declare that are relevant to the content of this article.

References

- Agrotis L, Schönemann E, Enderle W, et al (2017) The IGS Real Time Service. In: GNSS 2017—DVW-Seminar Kompetenz für die Zukunft. Potsdam
- Allan DW (1987) Time and frequency (time-domain) characterization, estimation, and prediction of precision clocks and oscillators. *IEEE Trans Ultrason Ferroelect, Freq Contr* 34:647–654. <https://doi.org/10.1109/T-UFFC.1987.26997>
- Allan DW, Weiss MA (1980) Accurate time and frequency transfer during common-view of a GPS satellite. In: 34th Annual symposium on frequency control. IEEE, pp 334–346
- Beard R, Senior K (2017) Clocks. In: Teunissen PJG, Montenbruck O (eds) Springer Handbook of global navigation satellite systems. Springer, Cham, pp 121–164
- Bock H, Dach R, Yoon Y, Montenbruck O (2009) GPS clock correction estimation for near real-time orbit determination applications. *Aerosp Sci Technol* 13:415–422. <https://doi.org/10.1016/j.ast.2009.08.003>
- Cerretto G, Tavella P, Lahaye F, et al (2011) PPP using NRCan ultra rapid products (EMU): near real-time comparison and monitoring of time scales generated in time and frequency laboratories. In: 2011 Joint conference of the IEEE international frequency control and the European frequency and time forum (FCS) proceedings. IEEE, San Francisco, pp 1–6
- Dai X, Gong X, Li C et al (2022) Real-time precise orbit and clock estimation of multi-GNSS satellites with undifferenced ambiguity resolution. *J Geod* 96:73. <https://doi.org/10.1007/s00190-022-01664-3>
- Defraigne P (2017) GNSS time and frequency transfer. In: Teunissen PJG, Montenbruck O (eds) Springer handbook of global navigation satellite systems. Springer, Cham, pp 1187–1206
- Defraigne P, Aerts W, Pottiaux E (2015) Monitoring of UTC(k)'s using PPP and IGS real-time products. *GPS Solut* 19:165–172. <https://doi.org/10.1007/s10291-014-0377-5>
- Gong X, Gu S, Lou Y et al (2018) An efficient solution of real-time data processing for multi-GNSS network. *J Geod* 92:797–809. <https://doi.org/10.1007/s00190-017-1095-x>
- Gong X, Zheng F, Gu S et al (2022) The long-term characteristics of GNSS signal distortion biases and their empirical corrections. *GPS Solut* 26:52. <https://doi.org/10.1007/s10291-022-01238-y>
- Gu S, Shi C, Lou Y, Liu J (2015) Ionospheric effects in uncalibrated phase delay estimation and ambiguity-fixed PPP based on raw observable model. *J Geod* 89:447–457. <https://doi.org/10.1007/s00190-015-0789-1>
- Gu S, Dai C, Fang W et al (2021) Multi-GNSS PPP/INS tightly coupled integration with atmospheric augmentation and its application in urban vehicle navigation. *J Geod* 95:64. <https://doi.org/10.1007/s00190-021-01514-8>
- Guo J, Xu X, Zhao Q, Liu J (2016) Precise orbit determination for quad-constellation satellites at Wuhan University: strategy, result validation, and comparison. *J Geod* 90:143–159. <https://doi.org/10.1007/s00190-015-0862-9>
- Guo W, Song W, Niu X et al (2019) Foundation and performance evaluation of real-time GNSS high-precision one-way timing system. *GPS Solut* 23:23. <https://doi.org/10.1007/s10291-018-0811-1>
- Guo W, Zuo H, Mao F et al (2022) On the satellite clock datum stability of RT-PPP product and its application in one-way timing and time synchronization. *J Geod* 96:52. <https://doi.org/10.1007/s00190-022-01638-5>
- Hauschild A, Montenbruck O (2009) Kalman-filter-based GPS clock estimation for near real-time positioning. *GPS Solut* 13:173–182. <https://doi.org/10.1007/s10291-008-0110-3>
- Hutsell ST (1995) Relating the Hadamard variance to MCS kalman filter clock estimation. In: Proceedings of the 27th annual precise time and time interval systems and applications meeting. San Diego, pp 291–302
- Hutsell ST, Reid WG, Mobbs HS (1996) Operational use of the hadamard variance in GPS. In: 28th Annual precise time and time interval (PTTI) systems and applications meeting. Reston, USA
- Kouba J, Héroux P (2001) Precise point positioning using IGS orbit and clock products. *GPS Solut* 5:12–28. <https://doi.org/10.1007/PL00012883>
- Lou Y, Gong X, Gu S et al (2017) Assessment of code bias variations of BDS triple-frequency signals and their impacts on ambiguity resolution for long baselines. *GPS Solut* 21:177–186. <https://doi.org/10.1007/s10291-016-0514-4>
- Luo X, Gu S, Lou Y et al (2020) Amplitude scintillation index derived from C/N0 measurements released by common geodetic GNSS receivers operating at 1 Hz. *J Geod* 94:27. <https://doi.org/10.1007/s00190-020-01359-7>
- Montenbruck O, Hugentobler U, Dach R et al (2012) Apparent clock variations of the Block IIF-1 (SVN62) GPS satellite. *GPS Solut* 16:303–313. <https://doi.org/10.1007/s10291-011-0232-x>
- Montenbruck O, Hauschild A, Häberling S et al (2017) High-rate clock variations of the Galileo IOV-1/2 satellites and their impact on carrier tracking by geodetic receivers. *GPS Solut* 21:43–52. <https://doi.org/10.1007/s10291-015-0503-z>
- Orgiazzi D, Tavella P, Lahaye F (2005) Experimental assessment of the time transfer capability of precise point positioning (PPP). In: Proceedings of the 2005 IEEE international frequency control symposium and exposition, 2005. IEEE, Vancouver, pp 337–345
- Petit G, Jiang Z (2008) GPS all in view time transfer for TAI computation. *Metrologia* 45:35–45. <https://doi.org/10.1088/0026-1394/45/1/006>
- Ren Z, Gong H, Lyu D et al (2023) Time transfer with BDS-3 signals: CV, PPP and IPPP. *Meas Sci Technol* 34:045007. <https://doi.org/10.1088/1361-6501/acaf96>
- Riley WJ (2008) Handbook of frequency stability analysis. National Institute of Standards and Technology, Gaithersburg
- Senior KL (2012) International GNSS Service technical report 2011—Report of the IGS working group on clock products. IGS
- Senior K, Koppang P, Ray J (2003) Developing an IGS time scale. *IEEE Trans Ultrason Ferroelectr Freq Control* 50:585–593. <https://doi.org/10.1109/TUFFC.2003.1209545>
- Senior KL, Ray JR, Beard RL (2008) Characterization of periodic variations in the GPS satellite clocks. *GPS Solut* 12:211–225. <https://doi.org/10.1007/s10291-008-0089-9>
- Shi C, Guo S, Gu S et al (2019) Multi-GNSS satellite clock estimation constrained with oscillator noise model in the existence of data discontinuity. *J Geod* 93:515–528. <https://doi.org/10.1007/s00190-018-1178-3>
- Stein SR, Filler RL (1988) Kalman filter analysis for real time applications of clocks and oscillators. In: Proceedings of the 42nd annual frequency control symposium, 1988. IEEE, Baltimore, pp 447–452
- van Bree RJP, Tiberius CCJM (2012) Real-time single-frequency precise point positioning: accuracy assessment. *GPS Solut* 16:259–266. <https://doi.org/10.1007/s10291-011-0228-6>

- Vannicola F, Beard R, White J, et al (2010) GPS block IIF atomic frequency standard analysis. pp 181–196
- Verhasselt K, Defraigne P (2019) Multi-GNSS time transfer based on the CGGTTS. *Metrologia* 56:065003. <https://doi.org/10.1088/1681-7575/ab3ed7>
- Yang X, Gu S, Gong X et al (2019) Regional BDS satellite clock estimation with triple-frequency ambiguity resolution based on undifferenced observation. *GPS Solut* 23:33. <https://doi.org/10.1007/s10291-019-0828-0>
- Zhang Z, Lou Y, Zheng F, Gu S (2021) ON GLONASS pseudo-range inter-frequency bias solution with ionospheric delay modeling and the undifferenced uncombined PPP. *J Geod* 95:32. <https://doi.org/10.1007/s00190-021-01480-1>
- Zheng F, Lou Y, Gu S et al (2018) Modeling tropospheric wet delays with national GNSS reference network in China for BeiDou precise point positioning. *J Geod* 92:545–560. <https://doi.org/10.1007/s00190-017-1080-4>
- Zumberge JF, Heflin MB, Jefferson DC et al (1997) Precise point positioning for the efficient and robust analysis of GPS data from large networks. *J Geophys Res Solid Earth* 102:5005–5017. <https://doi.org/10.1029/96JB03860>

Springer Nature or its licensor (e.g. a society or other partner) holds exclusive rights to this article under a publishing agreement with the author(s) or other rightsholder(s); author self-archiving of the accepted manuscript version of this article is solely governed by the terms of such publishing agreement and applicable law.